Supplement of Atmos. Chem. Phys. Discuss., 15, 35057–35115, 2015
http://www.atmos-chem-phys-discuss.net/15/35057/2015/
doi:10.5194/acpd-15-35057-2015-supplement
© Author(s) 2015. CC Attribution 3.0 License.

Atmospheric Chemistry and Physics Discussions

Supplement of

Influences of emission sources and meteorology on aerosol chemistry in a polluted urban environment: results from DISCOVER-AQ California

D. E. Young et al.

Correspondence to: Q. Zhang (dkwzhang@ucdavis.edu)

The copyright of individual parts of the supplement might differ from the CC-BY 3.0 licence.

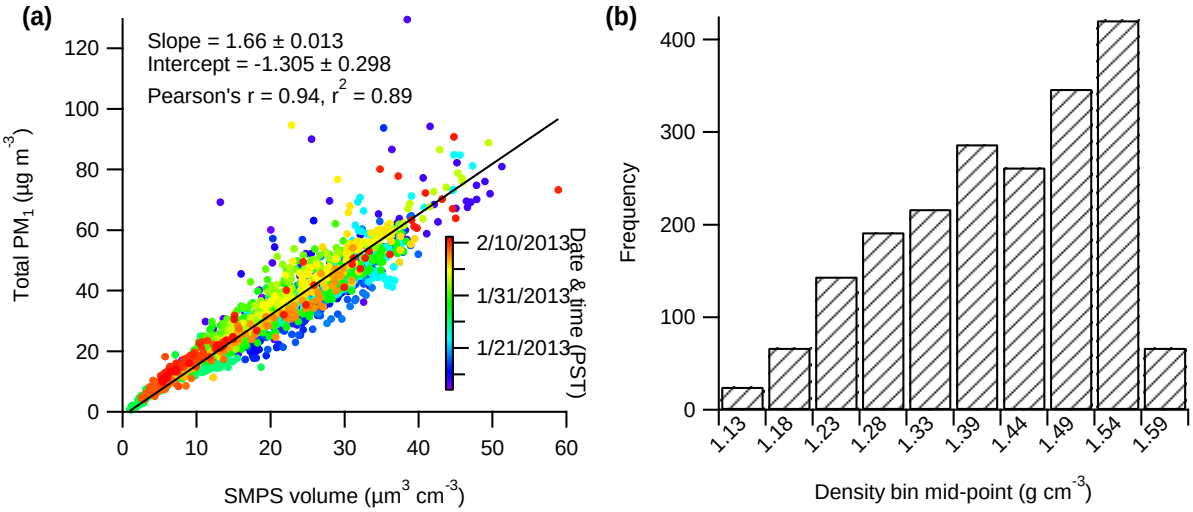

Figure S1. (a) Scatter plot of the total PM_1 mass (NR-PM_1 plus BC) versus SMPS volume, where the NR-PM_1 has been corrected using a time- and composition-dependent collection efficiency (Middlebrook et al., 2012); **(b)** histogram of particle density calculated based on PM_1 composition, which consists of ~34% ammonium nitrate (density = 1.72 g cm^{-3}), ~4.3% ammonium sulfate (density = 1.77 g cm^{-3}), ~1.6% ammonium chloride (density = 1.52 g cm^{-3}), ~33% POA (density = 1 g cm^{-3}), ~22% SOA (density = 1.27 g cm^{-3}), and ~4.8% BC (density = 1.8 g cm^{-3}), averaging 1.39 g cm^{-3}.

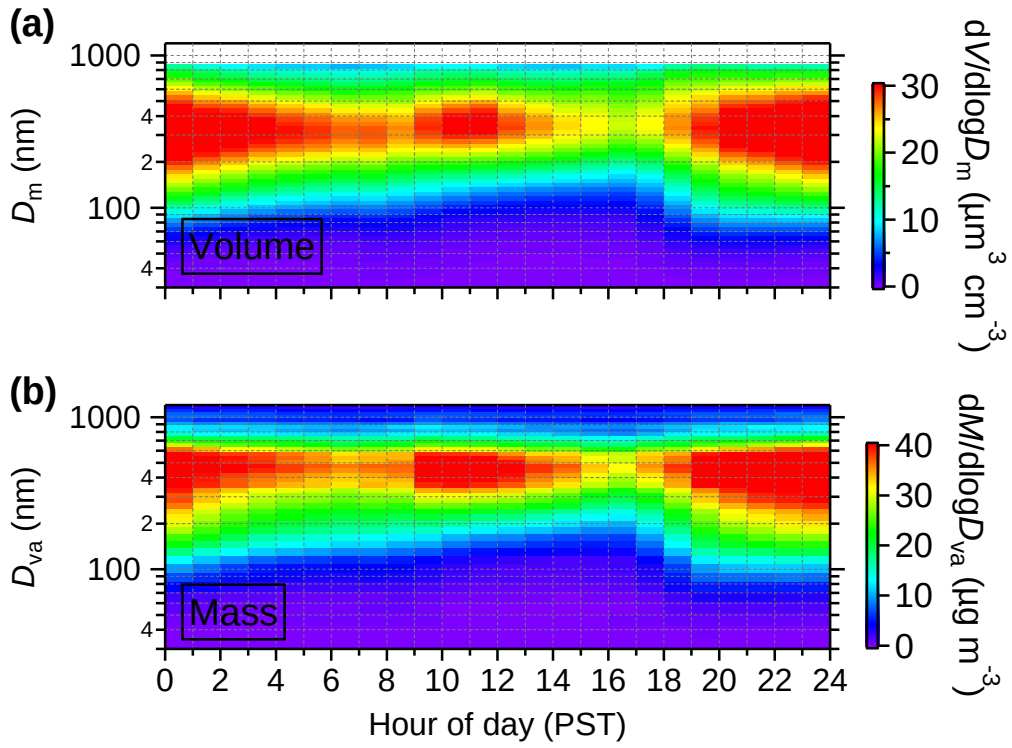

28

29 **Figure S2.** Diurnal variations of the size distribution of **(a)** volume from the SMPS (in mobility
30 diameter, D_m**)**; **(b)** NR-PM_1 mass from the AMS (in vacuum aerodynamic diameter, D_{va}).

31

Table S1. Comparison of the O/C, H/C, and OM/OC ratios of total OA and the six OA factors identified from PMF analysis calculated using the Aiken-Ambient method (Aiken et al., 2008) and the improved Canagaratna-Ambient method (Canagaratna et al., 2015).

Species	Ratio	Aiken-Ambient	Canagaratna-Ambient
OA	O/C	0.32	0.42
	H/C	1.54	1.70
	OM/OC	1.57	1.71
HOA	O/C	0.07	0.09
	H/C	1.95	2.10
	OM/OC	1.28	1.28
COA	O/C	0.15	0.19
	H/C	1.76	1.90
	OM/OC	1.35	1.42
BBOA1	O/C	0.25	0.33
	H/C	1.56	1.74
	OM/OC	1.48	1.60
BBOA2	O/C	0.43	0.60
	H/C	1.56	1.78
	OM/OC	1.72	1.94
SV-OOA	O/C	0.50	0.63
	H/C	1.55	1.70
	OM/OC	1.84	1.98
LV-OOA	O/C	0.69	0.90
	H/C	1.38	1.57
	OM/OC	2.05	2.33

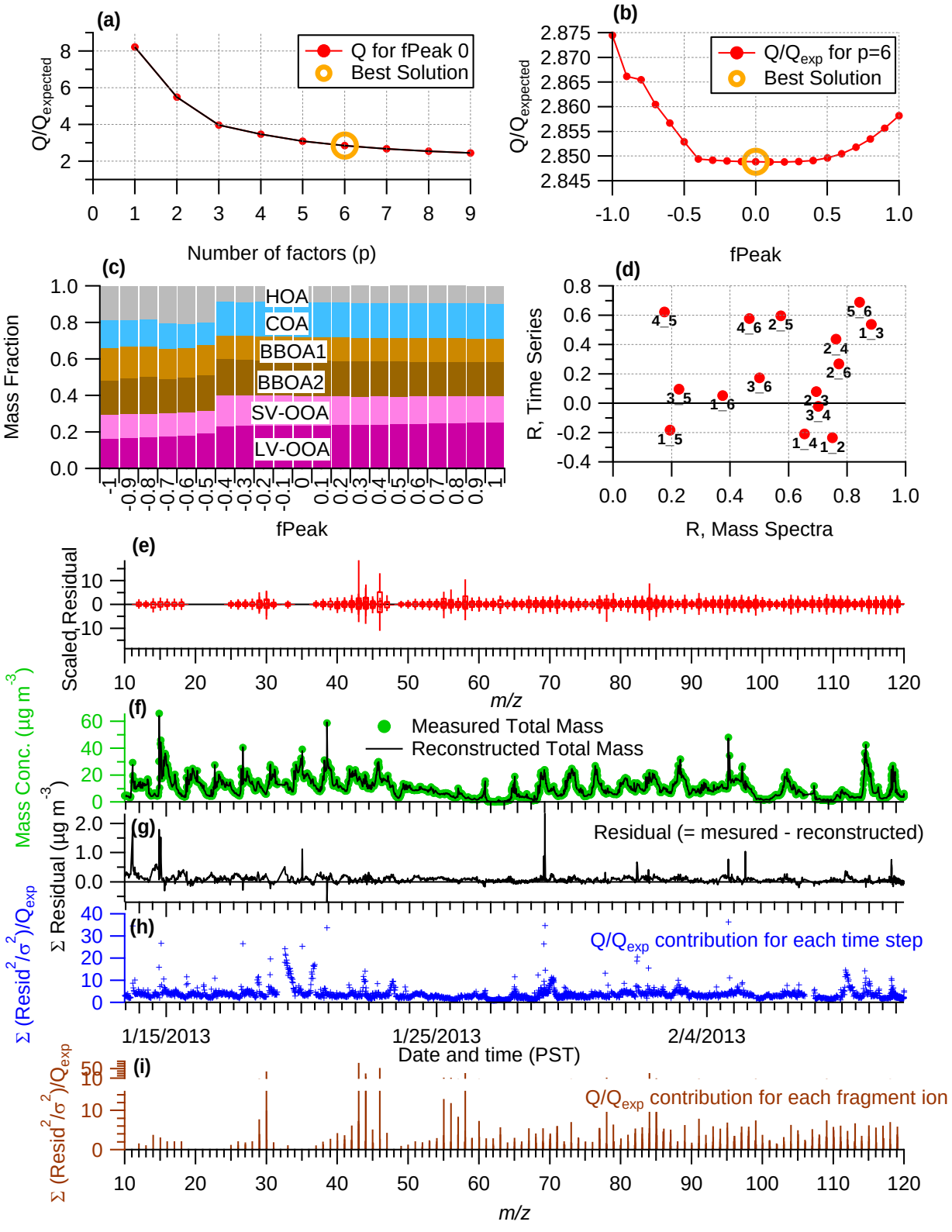

Figure S3. Summary of the key diagnostic plots of the chosen 6-factor solution from PMF analysis of the organic aerosol fraction: **(a)** Q/Q_{exp} as a function of the number of factors (p)

explored in PMF analysis, with the best solution denoted by the open orange circle. Plots **b-i** are for the chosen solution set, containing 6 factors: **(b)** Q/Q_{exp} as a function of fPeak; **(c)** mass fractional contribution to the total OA mass of each of the PMF factors, including the residual (in black), as a function of fPeak; **(d)** Pearson's r correlation coefficient values for correlations among the time series and mass spectra of the PMF factors. Here, 1 = LV-OOA, 2 = BBOA1, 3 = SV-OOA, 4 = BBOA2, 5 = HOA, and 6 = COA; **(e)** box and whiskers plot showing the distributions of scaled residuals for each *m/z*; **(f)** time series of the measured organic mass and the reconstructed organic mass from the sum of the six OA factors; **(g)** time series of the variations in the residual (= measured – reconstructed) of the fit; **(h)** the Q/Q_{exp} for each point in time; **(i)** the Q/Q_{exp} values for each fragment ion.

Table S2. Correlation coefficient (Pearson's r) for comparisons between the mass spectra of the OA factors derived in this study with reference mass spectra from Ng et al. (2010) and those determined from the winter 2010 campaign (Ge et al., 2012).

	Reference mass spectrum	Pearson's r	2010 campaign mass spectrum	Pearson's r
HOA	HOA	0.98	HOA	0.98
COA	COA*	0.95	COA	0.99
BBOA1	BBOA	0.94	BBOA	0.91
BBOA2	BBOA	0.90	BBOA	0.97
SV-OOA	SV-OOA	0.90	OOA	0.96
LV-OOA	LV-OOA	0.84	OOA	0.95

*COA mass spectrum from Allan et al. (2010).

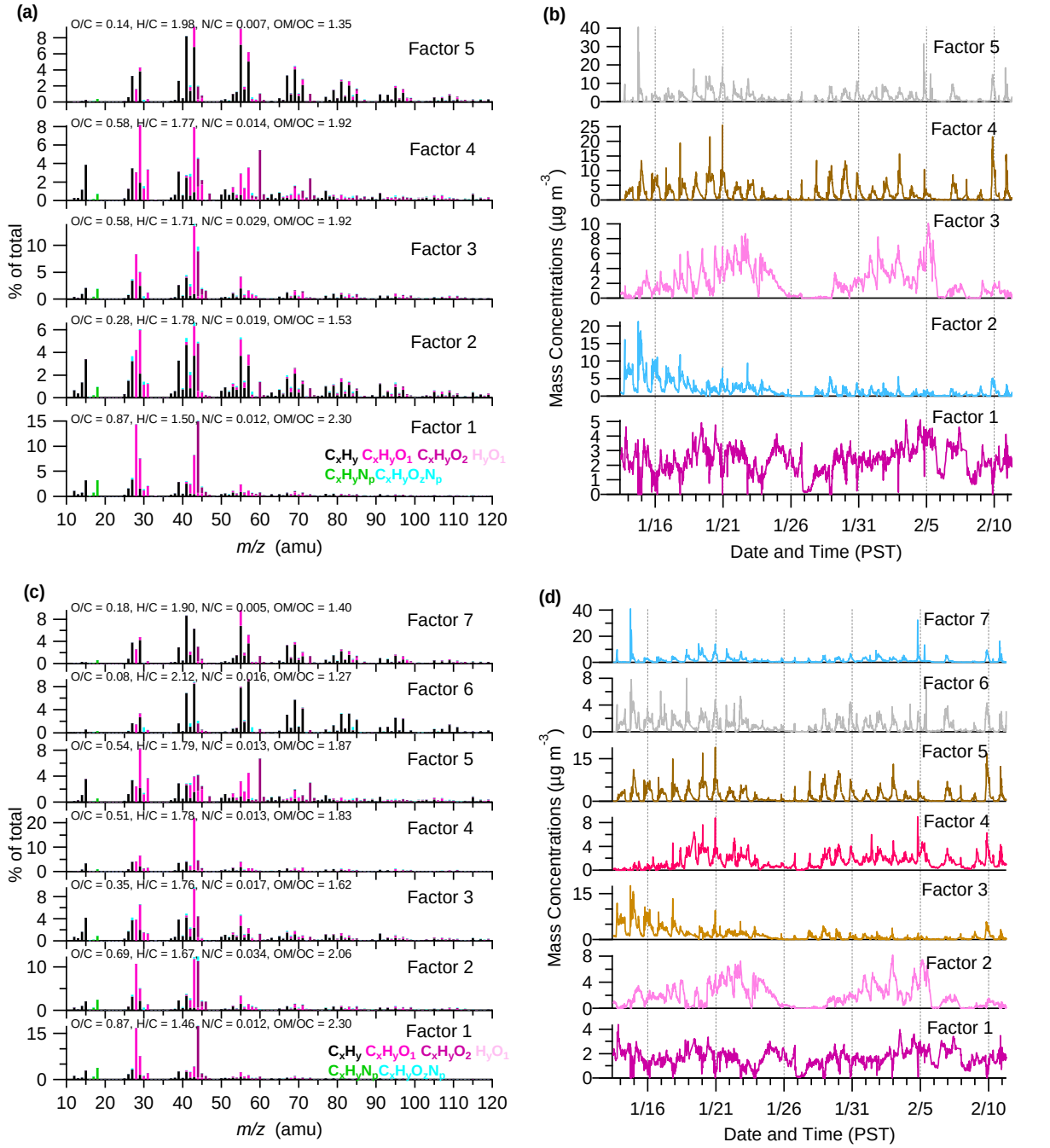

Figure S4. Overview of two other solution sets from PMF analysis: **(a)(b)** High resolution mass spectra and time series of the different OA factors from the 5-factor solution; **(c)(d)** High resolution mass spectra and time series of the different OA factors from the 7-factor solution. The mass spectra are colored by different ion families and the time series are colored by possible factor sources (grey = HOA, blue = COA, brown = BBOA, pink = OOA). See Sect. 2.3.2 in the main manuscript for a discussion on these solution sets.

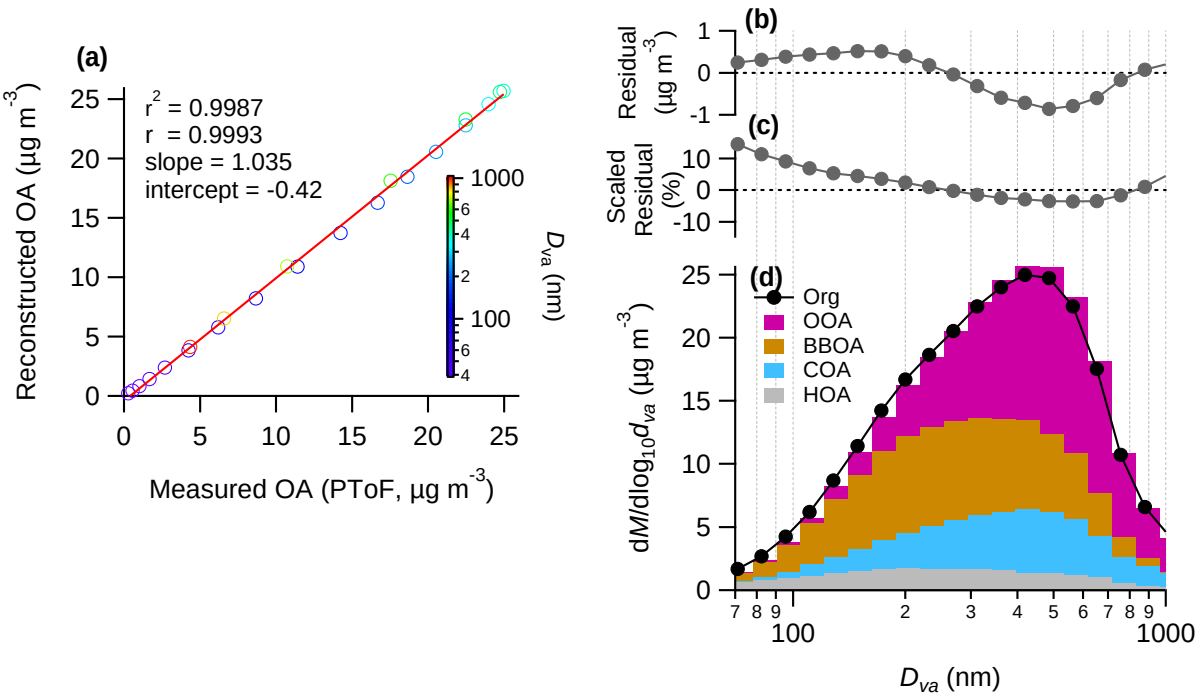

Figure S5. Summary of key diagnostics from the fitting of the derived size distributions of the four main OA factors: **(a)** scatter plot of the reconstructed vs. measured OA mass concentration for each size bin (40-1200 nm); **(b)** absolute residual of the reconstructed compared to the measured OA mass concentration for each size bin; **(c)** scaled residual of the reconstructed compared to the measured OA mass concentration for each size bin; and **(d)** stacked size distributions of the OA factors and the total measured organic aerosol size distribution.

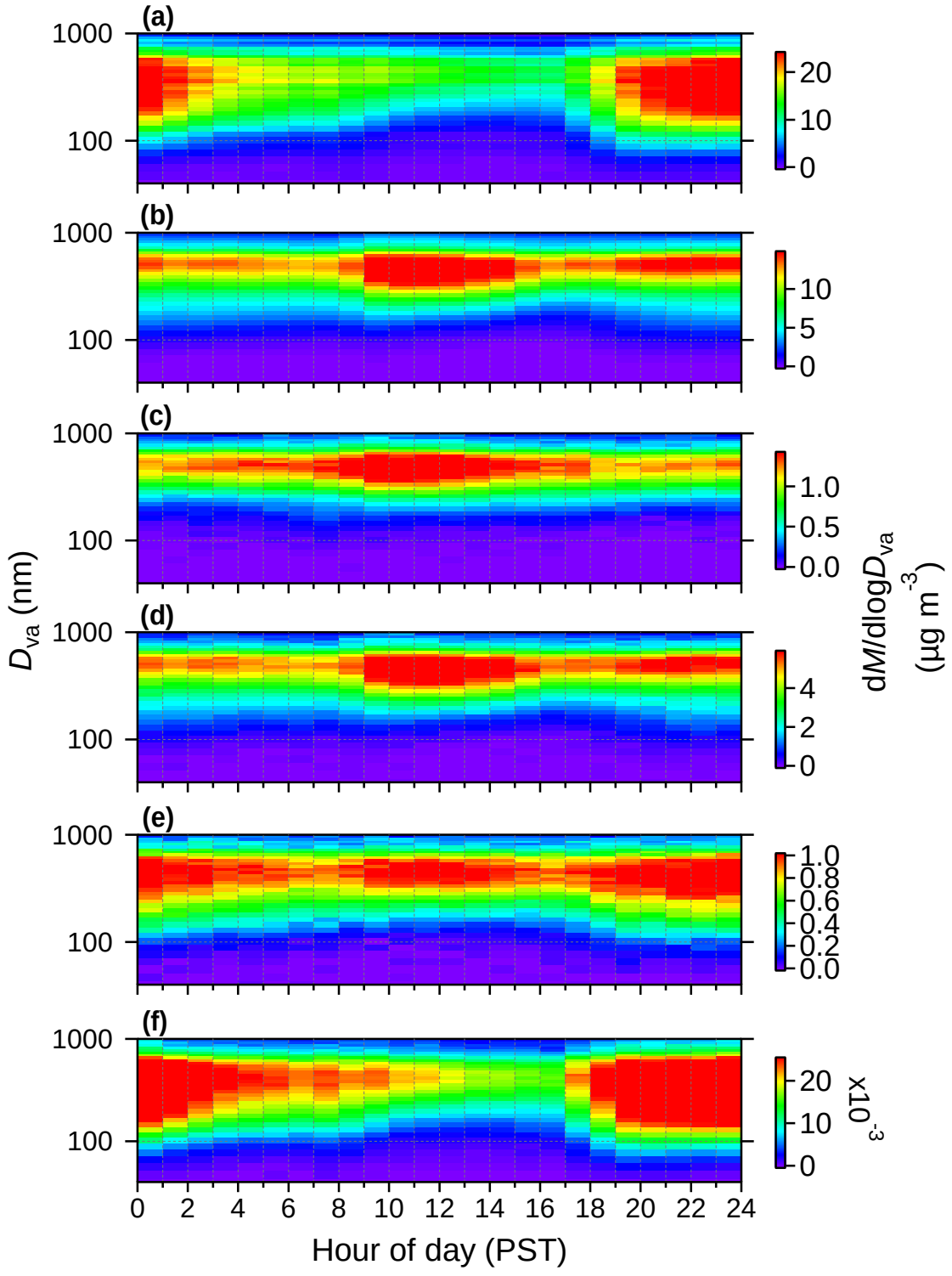

67

68 **Figure S6.** Diurnal variations of mass-based size distributions of **(a)** organics; **(b)** nitrate; **(c)**
69 sulfate; **(d)** ammonium; **(e)** Org44 as a tracer for secondary organic aerosols; and **(f)** Org41 as a
70 tracer for hydrocarbon containing aerosols.

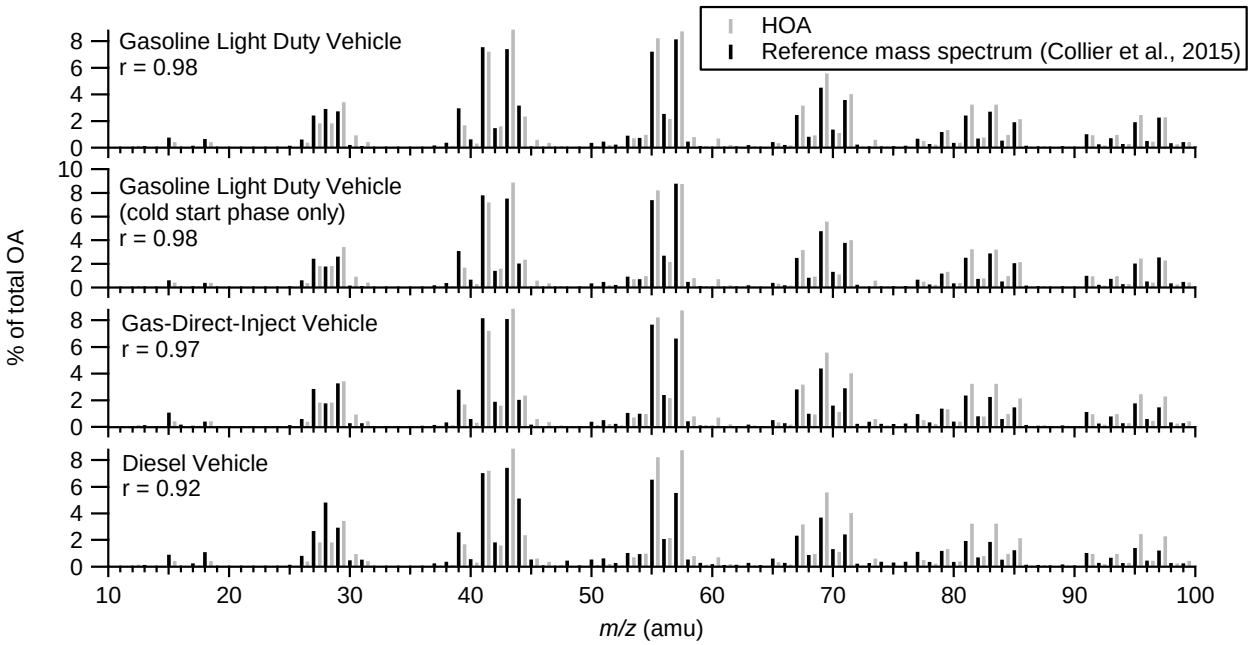

Figure S7. Comparison of the HOA mass spectrum from the current study and mass spectra of different types of vehicles from a vehicle emissions study (Collier et al., 2015).

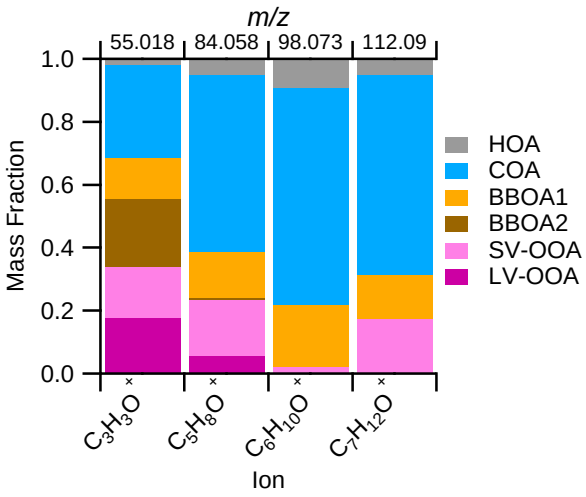

75

76 **Figure S8.** Mass fractional contribution of the six OA factors from PMF analysis to various ions.

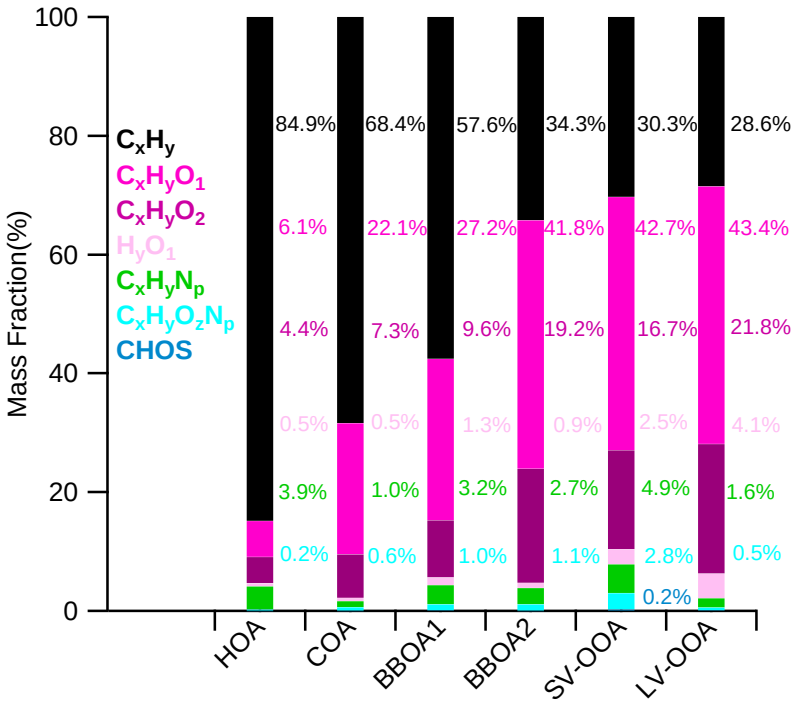

77

78 **Figure S9.** Average mass fractional contributions of seven ion families to each of the OA

79 factors.

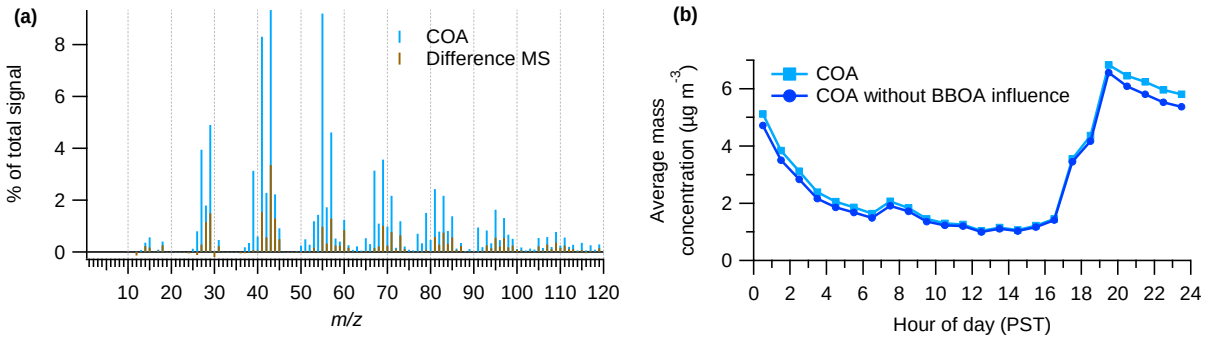

Figure S10. (a) Mass spectra of COA and the difference of between COA from 2013 and 2010 (after scaling the 2013 COA mass spectrum (MS) based on the ratio between $C_3H_3O^+$ in 2010 and 2013) and **(b)** Average diurnal profiles of the COA derived from PMF analysis and COA with the influence of BBOA removed (see Sect. 3.2.3 for more details).

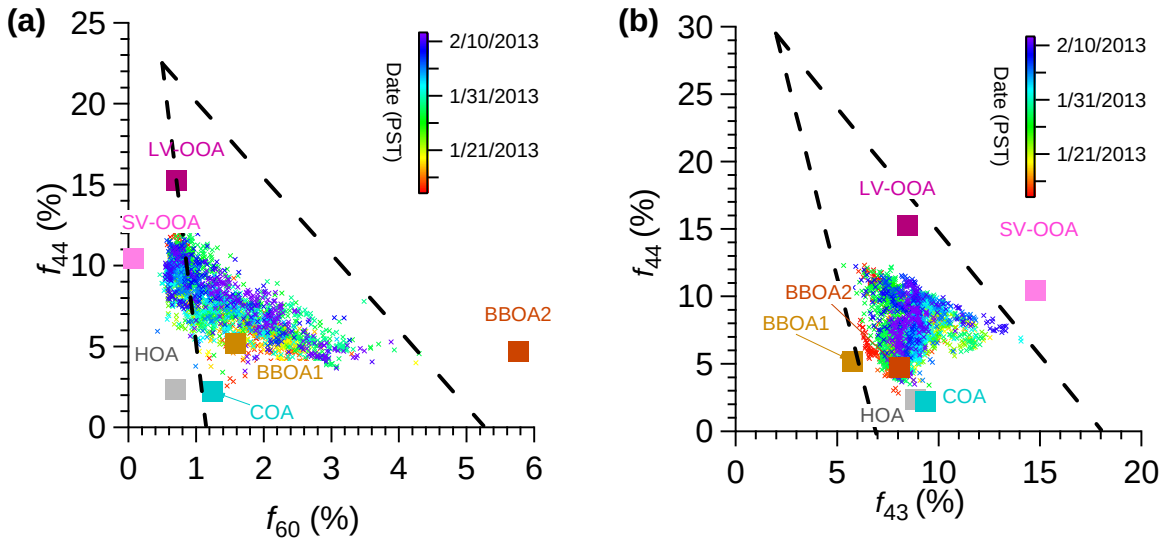

Figure S11. Triangle plots of **(a)** f_{44} vs. f_{60} and **(b)** f_{44} vs. f_{43} for the six OA factors and all measured OA data (dots), colored by time of the day. f_{44}, f_{60}, and f_{43} are the ratios of the organic signal at *m/z* = 44, 60, and 43 to the total organic signal in the component mass spectrum, respectively. The triangular space in (a) is used to investigate the evolution of BBOA and was proposed by Cubison et al. (2011). In this study BBOA1 locates at the lower left corner whereas BBOA2 locates outside of the triangle on the right due to its high *m/z* 60 signal. The triangular space in (b) is used to investigate the evolution of OA, particularly OOA. OOA is typically observed to fall into a well-defined triangular region within which SV-OOA and LV-OOA tend to occupy discrete regions, thus it is suggested that SV-OOA represents fresh SOA with low f_{44} and LV-OOA represents aged and highly oxidized OA, with high f_{44}. It has been observed that fresh SOA becomes increasingly oxidized and less volatile through additional processing in the atmosphere resulting in LV-OOA, thus the evolution of SOA is regarded as a continuum of oxidation.

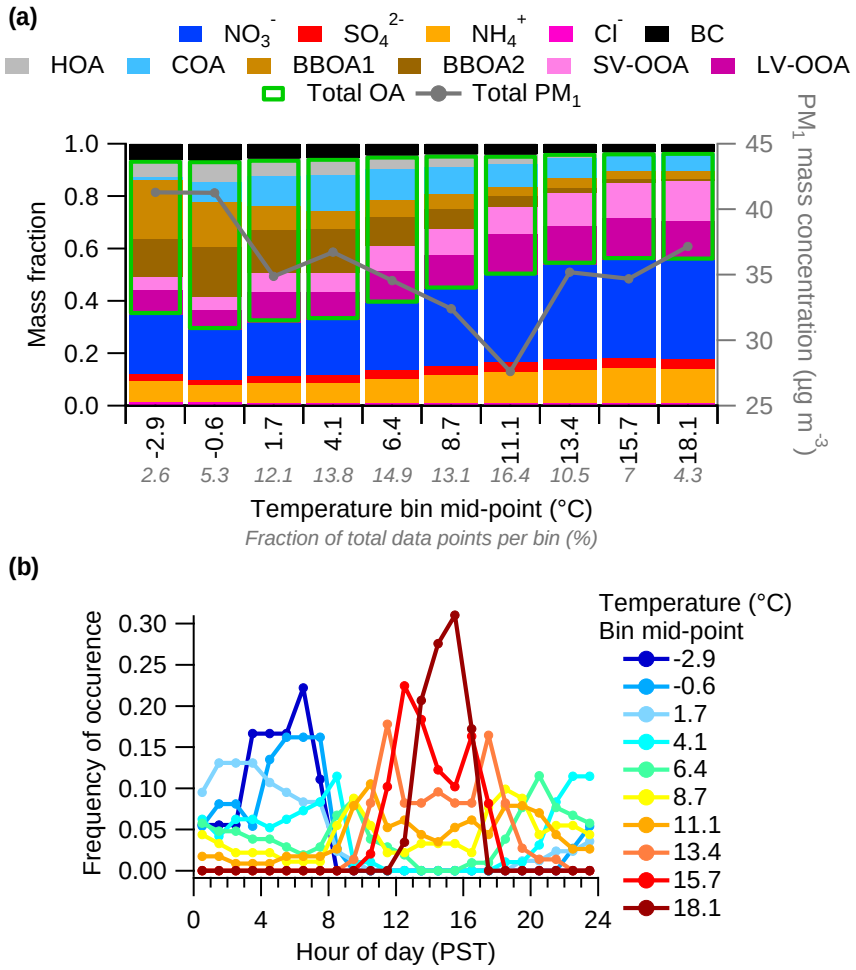

Figure S12. (a) Mass fractional contribution to total PM_1 of the non-refractory secondary inorganic species (nitrate (NO_3^-), sulfate (SO_4^{2-}), ammonium (NH_4^+), chloride (Cl^-)), black carbon (BC), and the six OA factors (hydrocarbon-like OA (HOA), cooking OA (COA), biomass burning OA 1 (BBOA1), biomass burning OA 2 (BBOA2), semi-volatile oxygenated OA (SV-OOA), low volatility oxygenated OA (LV-OOA)) as a function of temperature during the whole campaign and average total PM_1 as a function of temperature; **(b)** frequency of occurrence of the temperature bins in plot (a) as a function of hour of the day.

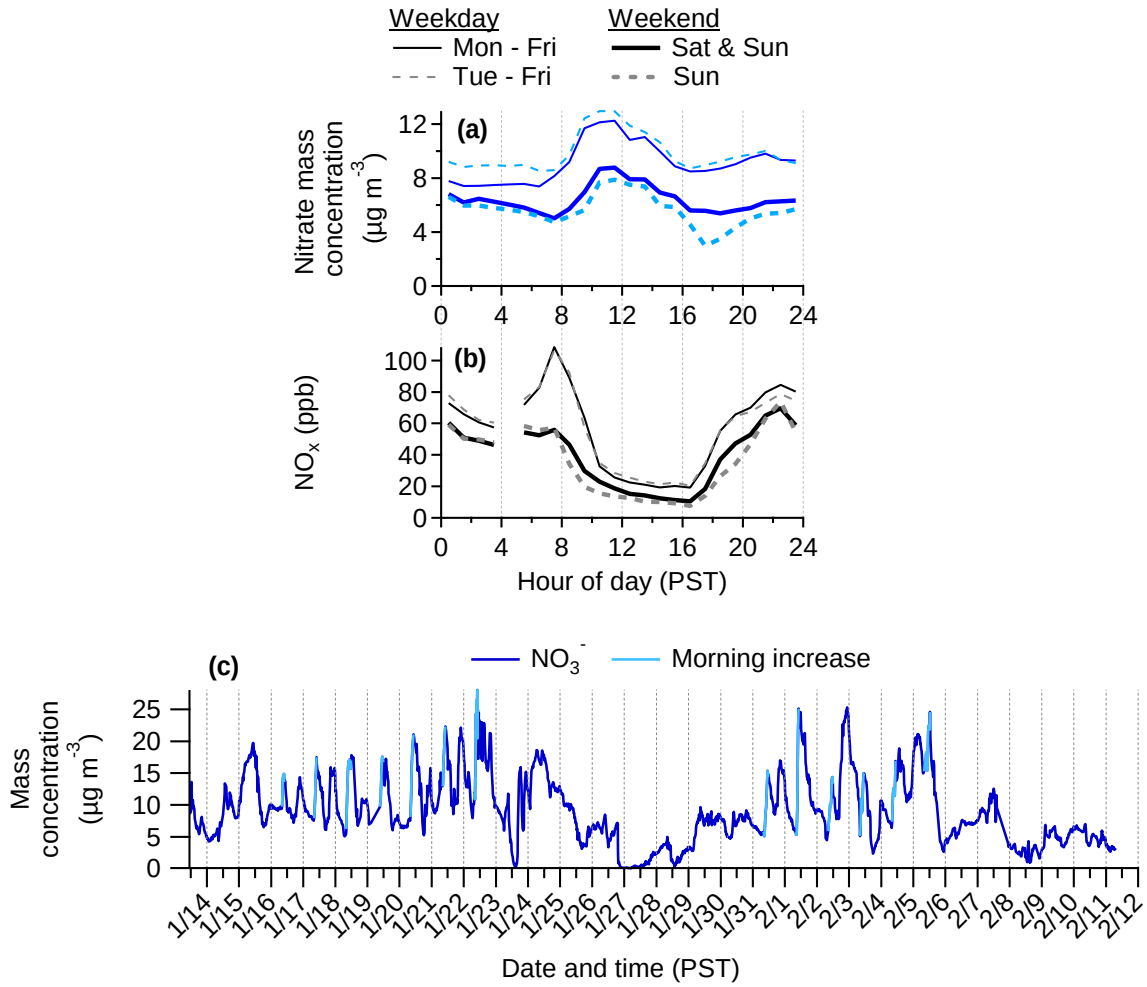

Figure S13. Average diurnal mass concentrations when different definitions of weekdays and weekends are used for **(a)** nitrate and **(b)** NO_x, a gaseous precursor of particulate nitrate. **(c)** Time series of nitrate highlighted with the occasions when a rapid increase in concentration during the morning is observed.

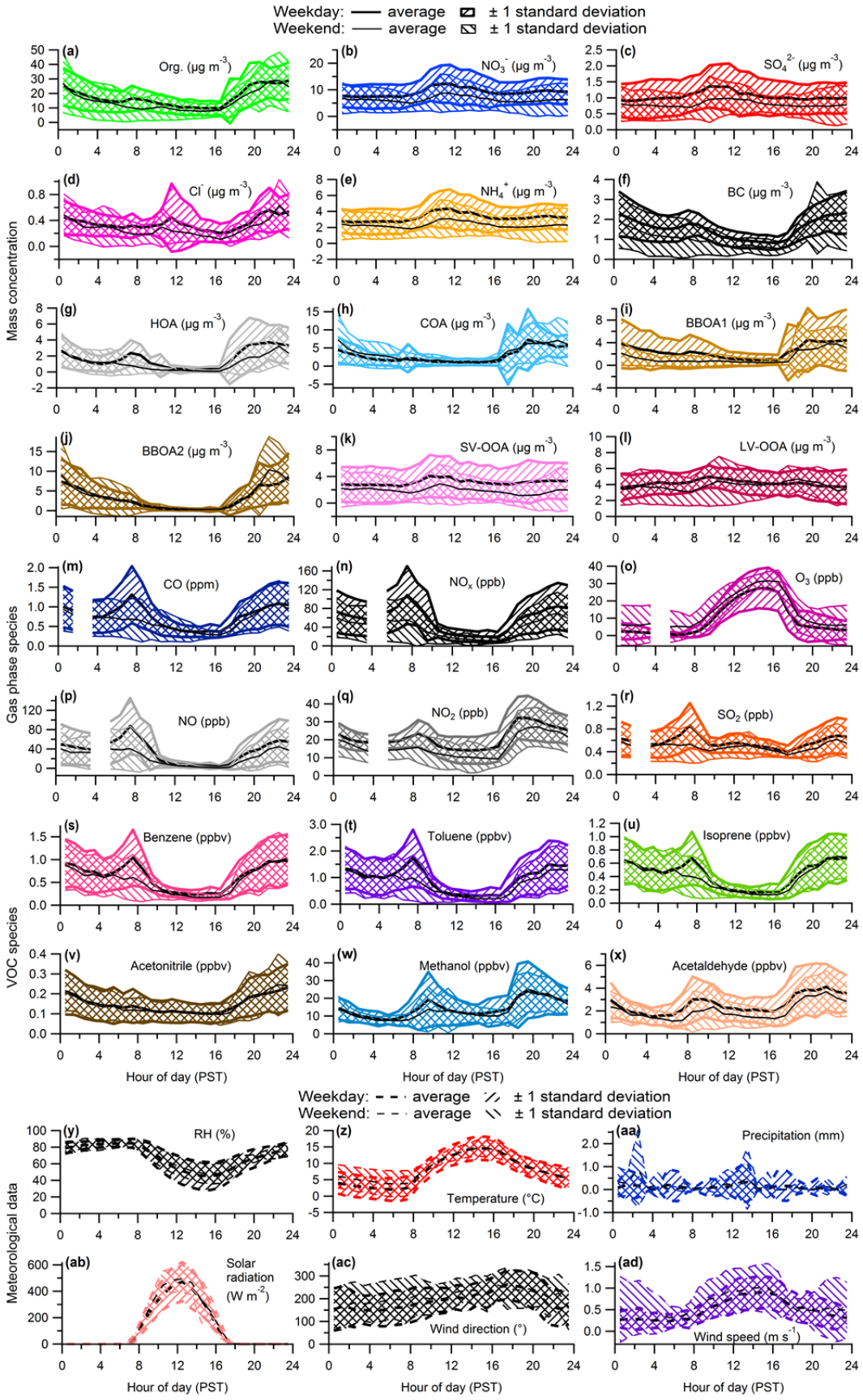
Weekday: average ± 1 standard deviation
Weekend: average ± 1 standard deviation
(a) Org. (μg m-3)
(b) NO3- (μg m-3)
(c) SO4 2- (μg m-3)
(d) Cl- (μg m-3)
(e) NH4+ (μg m-3)
(f) BC (μg m-3)
(g) HOA (μg m-3)
(h) COA (μg m-3)
(i) BBOA1 (μg m-3)
(j) BBOA2 (μg m-3)
(k) SV-OOA (μg m-3)
(l) LV-OOA (μg m-3)
Mass concentration
(m) CO (ppm)
(n) NOx (ppb)
(o) O3 (ppb)
(p) NO (ppb)
(q) NO2 (ppb)
(r) SO2 (ppb)
Gas phase species
(s) Benzene (ppbv)
(t) Toluene (ppbv)
(u) Isoprene (ppbv)
(v) Acetonitrile (ppbv)
(w) Methanol (ppbv)
(x) Acetaldehyde (ppbv)
VOC species
Hour of day (PST)
Weekday: average ± 1 standard deviation
Weekend: average ± 1 standard deviation
(y) RH (%)
(z) Temperature (°C)
(aa) Precipitation (mm)
(ab) Solar radiation (W m-2)
(ac) Wind direction (°)
(ad) Wind speed (m s-1)
Meteorological data
Hour of day (PST)

Figure S14. Diurnal profiles of **(a-f)** PM_1 species, **(g-l)** OA factors from PMF analysis, **(m-r)** various gas-phase species from the CARB monitoring station, **(s-x)** several VOCs measured by the PTR-TOF-MS, and **(v-ad)** various meteorological parameters. In all plots, thick lines relate to weekday diurnal variables and thin lines relate to weekend diurnal variables. Black lines represent the average diurnal profile with the hatched pattern denotes the ± one standard deviation.

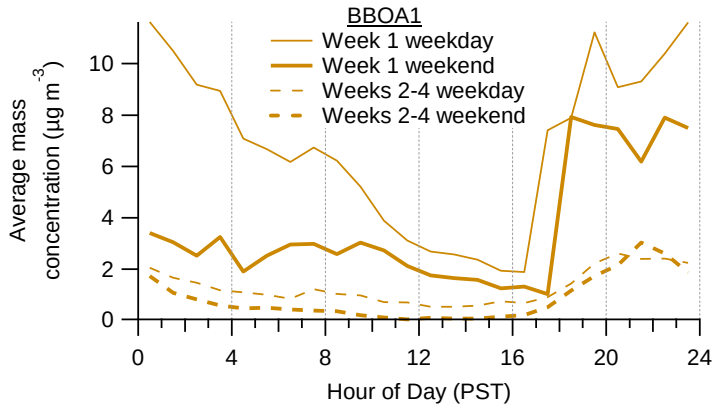

Figure S15. Average mass concentration diurnals for BBOA1 for the weekday and weekends for the first week of the campaign and weeks 2-4.

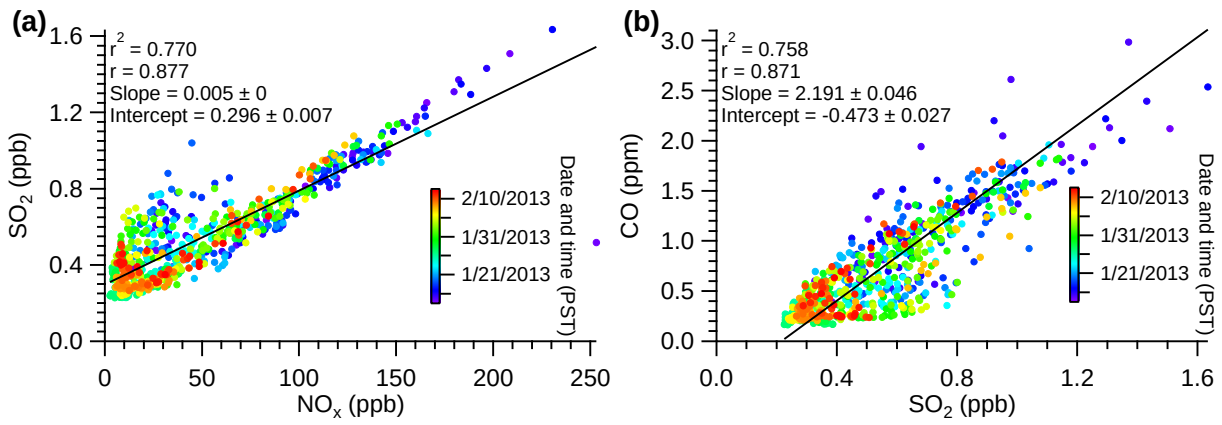

124

125 **Figure S16.** Scatter plots between various gas-phase species: **(a)** SO_2 vs. NO_x, which are
126 gaseous precursors to particulate sulfate and nitrate, respectively; and **(b)** CO vs. SO_2, where CO
127 is used as an indicator for boundary layer dynamics.

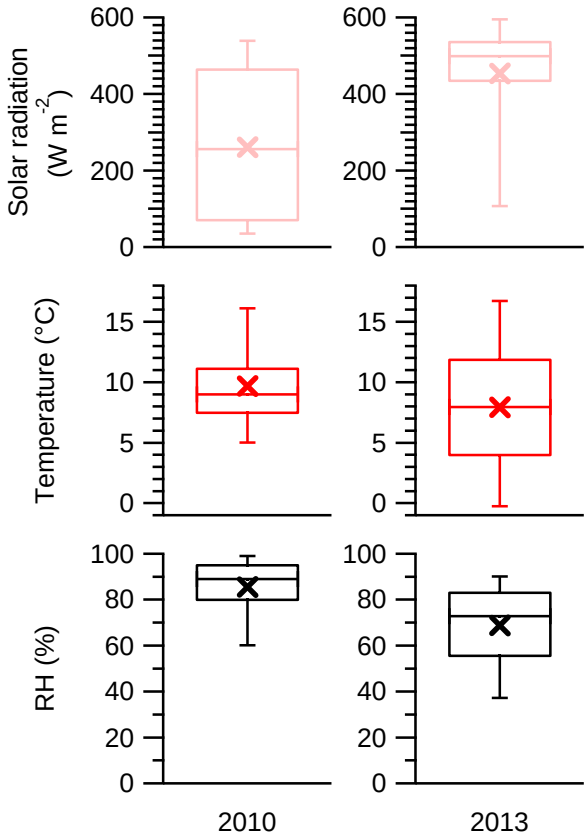

Figure S17. Box and whisker plots of solar radiation, temperature and RH for the winter 2010 and 2013 campaigns. Solar radiation data plotted here are for the daytime peak between 12:00 and 13:00 for both years. The 95th and 5th percentiles are denoted by the whiskers above and below the boxes, the 75th and 25th percentiles are denoted by the top and bottom of the boxes, the median values are denoted by the horizontal line within the box, and the mean values are denoted by the cross markers.

References

Aiken, A. C., Decarlo, P. F., Kroll, J. H., Worsnop, D. R., Huffman, J. A., Docherty, K. S., Ulbrich, I. M., Mohr, C., Kimmel, J. R., Sueper, D., Sun, Y., Zhang, Q., Trimborn, A., Northway, M., Ziemann, P. J., Canagaratna, M. R., Onasch, T. B., Alfarra, M. R., Prévôt, A. S. H., Dommen, J., Duplissy, J., Metzger, A., Baltensperger, U., and Jimenez, J. L.: O/C and OM/OC ratios of primary, secondary, and ambient organic aerosols with high-resolution time-of-flight aerosol mass spectrometry, Environmental science & technology, 42, 4478-4485, 2008.

Allan, J. D., Williams, P. I., Morgan, W. T., Martin, C. L., Flynn, M. J., Lee, J., Nemitz, E., Phillips, G. J., Gallagher, M. W., and Coe, H.: Contributions from transport, solid fuel burning and cooking to primary organic aerosols in two UK cities, Atmos. Chem. Phys., 10, 647-668, 2010.

Canagaratna, M. R., Jimenez, J. L., Kroll, J. H., Chen, Q., Kessler, S. H., Massoli, P., Hildebrandt Ruiz, L., Fortner, E., Williams, L. R., Wilson, K. R., Surratt, J. D., Donahue, N. M., Jayne, J. T., and Worsnop, D. R.: Elemental ratio measurements of organic compounds using aerosol mass spectrometry: characterization, improved calibration, and implications, Atmospheric Chemistry and Physics, 15, 253-272, 2015.

Collier, S., Zhou, S., Kuwayama, T., Forestieri, S., Brady, J., Zhang, M., Kleeman, M., Cappa, C., Bertram, T., and Zhang, Q.: Organic PM Emissions from Vehicles: Composition, O/C Ratio, and Dependence on PM Concentration, Aerosol Science and Technology, 49, 86-97, 2015.

Cubison, M. J., Ortega, A. M., Hayes, P. L., Farmer, D. K., Day, D., Lechner, M. J., Brune, W. H., Apel, E., Diskin, G. S., Fisher, J. A., Fuelberg, H. E., Hecobian, A., Knapp, D. J., Mikoviny, T., Riemer, D., Sachse, G. W., Sessions, W., Weber, R. J., Weinheimer, A. J., Wisthaler, A., and Jimenez, J. L.: Effects of aging on organic aerosol from open biomass burning smoke in aircraft and laboratory studies, Atmospheric Chemistry and Physics, 11, 12049-12064, 2011.

Ge, X., Setyan, A., Sun, Y., and Zhang, Q.: Primary and secondary organic aerosols in Fresno, California during wintertime: Results from high resolution aerosol mass spectrometry, Journal of Geophysical Research: Atmospheres, 117, n/a-n/a, 2012.

Middlebrook, A. M., Bahreini, R., Jimenez, J. L., and Canagaratna, M. R.: Evaluation of Composition-Dependent Collection Efficiencies for the Aerodyne Aerosol Mass Spectrometer using Field Data, Aerosol Science and Technology, 46, 258-271, 2012.

Ng, N. L., Canagaratna, M. R., Zhang, Q., Jimenez, J. L., Tian, J., Ulbrich, I. M., Kroll, J. H., Docherty, K. S., Chhabra, P. S., Bahreini, R., Murphy, S. M., Seinfeld, J. H., Hildebrandt, L., Donahue, N. M., DeCarlo, P. F., Lanz, V. A., Prévôt, A. S. H., Dinar, E., Rudich, Y., and Worsnop, D. R.: Organic aerosol components observed in Northern Hemispheric datasets from Aerosol Mass Spectrometry, Atmospheric Chemistry and Physics, 10, 4625-4641, 2010.